

Supersonic kinks and solitons in active solids

N.Gorbushin and L. Truskinovsky

*Laboratoire de Physique et Mécanique des Milieux Hétérogènes (PMMH UMR 7636) CNRS,
ESPCI Paris, PSL Research University, 10 rue Vauquelin, 75005 Paris, France*

Abstract

To show that steadily propagating nonlinear waves in active matter can be driven internally, we develop a prototypical model of a topological kink moving with a constant supersonic speed. We use a model of a bi-stable mass-spring (FPU) chain capable of generating active stress. In contrast to subsonic kinks in passive bi-stable chains, that are necessarily dissipative, the obtained supersonic solutions are purely anti-dissipative. Our numerical experiments point towards stability of the obtained kink-type solutions and the possibility of propagating kink-anti-kink bundles reminiscent of solitons. We show that even the simplest quasi-continuum approximation of the discrete model captures the most important features of the predicted active phenomena.

Keywords: Transition waves, chain model, active processes, metamaterials.

1 Introduction

Recently, considerable efforts have been focused on the modeling of active matter. We use this general term to describe a collection of interacting active agents, each one driven by its own internally fuelled mechanism [1, 2, 3, 4]. An important question concerns nucleation and propagation of transition fronts in such systems which can be modeled as *kinks* separating passive and active phases.

It was found that in various systems of self-propelled active objects, ranging from microorganisms to swarming robots, the transition from random to coherent motion is indeed accompanied by the formation of sharp transition zones. They were observed to be moving with particular velocities whose selection principle still remains an open problem [5, 6]. Most of the related theoretical work was done using various coarse grained versions of the discrete Vicsek model where active agents are postulated to move with particular speeds.

In this paper we study kink-type solutions, imitating transition fronts, in a different model of active matter which, instead of supporting active velocities, is able to generate locally active stresses. The known continuum models of active media with internally generated active stresses range from fluids [7, 8] to solids [9, 10, 11, 12]. Behind these models is the idea of chemo-mechanical coupling [13] with active stress emerging constitutively from the cross term linking a scalar chemical reaction with a tensorial mechanical action. For instance, in active gel theory the coupling is accomplished through an additional liquid-crystal-type vector field describing local polarization.

To achieve analytical transparency we neglect the chemical fuelling side of the problem and disregard polarization, assuming that the prescribed active stress is hydrostatic. If we limit our description to 1D but, in view of the anomalous softness of the associated phases, keep the inertial terms, we can write the ensuing continuum problem for the displacement field $u(x, t)$ in the form:

$$\rho \frac{\partial^2 u}{\partial t^2} = \frac{\partial \sigma}{\partial x}, \quad (1.1)$$

where we denoted by ρ the constant reference mass density. The activity is hidden in the constitutive relation for the stress σ which we assume to be elastic and represented by two branches: passive,

$$\sigma = E\varepsilon,$$

where $\varepsilon(x, t) = \partial u(x, t)/\partial x$ is the strain and E is the elastic modulus, and active,

$$\sigma = E\varepsilon + \sigma_0,$$

where $\sigma_0 > 0$ is the active stress which is fixed. The corresponding branches of the energy density are: $\phi = (E/2)\varepsilon^2$ (passive) and $\phi(\varepsilon) = (E/2)\varepsilon^2 + \sigma_0(\varepsilon - \varepsilon_c) + \Delta$ (active). Here, we introduced the critical strain ε_c where the transition from passive to active branch takes place; such transition requires energy expenditure (see Fig. 1):

$$\Delta = \sigma_0\varepsilon_c + \frac{\sigma_0^2}{2E},$$

which is assumed to be supplied actively at the microscopic level.

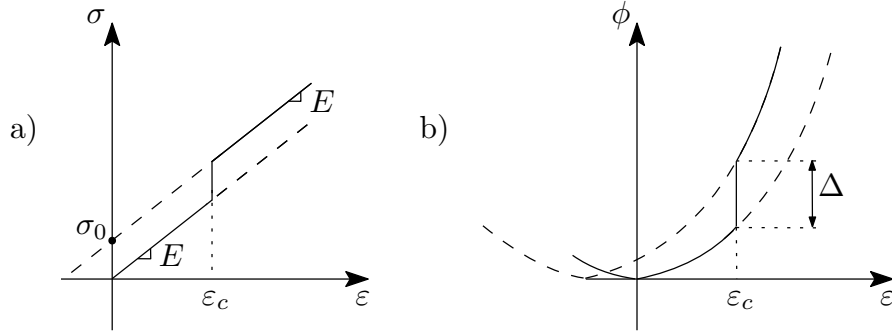


Figure 1: Constitutive behavior of a continuum element which can undergo a transition from passive $\varepsilon < \varepsilon_c$ to active $\varepsilon > \varepsilon_c$ regime: (a) stress-strain relation $\sigma = \sigma(\varepsilon)$, (b) free energy $\phi = \phi(\varepsilon)$.

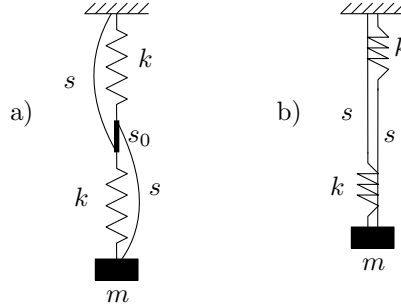


Figure 2: The mechanical model illustrating the Braess paradox [14]. When the link s_0 is cut the structure transform series to parallel arrangement of springs and the mass is lifted.

To show that the resulting material model is microscopically meaningful, consider a mechanical structure proposed in [14] as an application of the Braess paradox from the game theory [15]. The system includes two elastic springs with elasticity k and initial length a , two supporting inextensible elements with the length s , a linking inextensible element with the length s_0 and a mass m , see Fig. 2. When the string s_0 is cut the mass is lifted by the amount $s_0 - s + a + 3mg/(2k)$, where g is the acceleration of gravity (the spring connection transforms from series to parallel). The model depicted in Fig. 1 can be viewed as a stylized version of this mechanical system with the series arrangement describing the passive branch of the constitutive relation while the parallel arrangement corresponding to the active branch. The latter 'generates' extra stress which ultimately lifts the load.

Note that the transition to the active branch requires energy expenditure because the implied cutting ultimately involves bond breaking. The corresponding energy "cost" is characterized in our model by the parameter Δ and the required work can be viewed as produced by active forces implicitly present in the system. We note that the idea of [14] was recently used in [16] to build a passive metamaterial with negative compressibility. The interpretation of such material as active implies the presence of an active agent inserting the energy into the system each time the passive element reaches the critical strain and extracting it when the active material transforms back into its passive state; for a passive model where microscopically stored energy is used to push a propagating front see [17].

The focus of this paper is on velocity *selection* for the switching waves transforming the passive (analog of Vicsek's disordered) state into the active (analog of of Vicsek's ordered) state. Such waves are similar to the topological kinks in passive bi-stable materials except that they are not driven externally, by the applied stress biasing the double well potential, but internally, as a result of the energy consumption from the macroscopically invisible out of equilibrium chemical reservoir.

We first use the classical continuum theory to show that such kinks are necessarily supersonic and that their velocity remains undefined unless the microscopic problem is solved first. We then solve analytically the corresponding discrete problem for a bi-stable FPU (Fermi-Pasta-Ulam) chain [18] and obtain the required kinetic relation explicitly. It turns out to be universal but trivial.

More precisely, in contrast to subsonic kinks in a passive bi-stable FPU system that are necessarily dissipative, the obtained supersonic kinks are dissipation free. Our numerical experiments point towards stability of such waves. We also show the possibility of propagating kink-anti-kink bundles reminiscent of solitons and show that such active solitary waves indeed collide almost elastically. We also check that the simplest quasi-continuum approximation of the discrete model captures the most important features of the active kink propagation phenomenon both qualitatively and quantitatively.

Our main technical tool is the Fourier transform which can be used in this nonlinear problem due to the piece-wise linear, equal moduli approximation of the bi-stable constitutive relation. Similar approaches have been previously used for the description of the transition waves in passive FPU type systems [19, 20, 21]. To treat the case of different moduli, we could have used only slightly more complex approach based on the Wiener-Hopf method [22, 23], however, we have checked that such augmentation of the model does not change any of our main results.

The paper is organized as follows. In § 2, we introduce a continuum model and show that it produces non-unique solutions and does not select a particular kink velocity. In § 3, we develop the discrete model and solve it explicitly. We then show numerically the stability of the obtained solutions. The simplest quasi-continuum approximation of the discrete model is developed in § 4. Finally, in § 5, we present numerical evidence that kinks and anti-kinks can bundle together to form soliton like localized solutions. We present our conclusions in § 6. The solutions describing analytically tractable kinks in the linear discrete problem are presented in appendix A.

2 Continuum model

Staying within the continuum setting, we can rewrite our second order dynamic equation (1.1) as the first order system:

$$\frac{\partial \varepsilon}{\partial t} = \frac{\partial v}{\partial x}, \quad \rho \frac{\partial v}{\partial t} = \frac{\partial \sigma(\varepsilon)}{\partial x}, \quad (2.1)$$

where $v(x, t) = \partial u(x, t) / \partial t$ is the velocity field and

$$\sigma(\varepsilon) = \begin{cases} E\varepsilon, & \varepsilon < \varepsilon_c, \\ E\varepsilon + \sigma_0, & \varepsilon > \varepsilon_c \end{cases} \quad (2.2)$$

is the stress-strain relation. We are interested in the behavior of sharp discontinuities mimicking (diffuse) transition fronts. On the corresponding fronts the equations of elastodynamics (2.1) have to be

supplemented by the Rankine-Hugoniot jump conditions:

$$[[v]] + V[[\varepsilon]] = 0, \quad \rho V[[v]] + [[\sigma(\varepsilon)]] = 0, \quad (2.3)$$

where $[[f]] \equiv f_+ - f_-$ is the difference between the limiting values f_+ and f_- of a function $f(x)$ from the the right and left of the discontinuity.

While the phenomena in the bulk described by the system (2.1) are necessarily non-dissipative, discontinuities may serve as potential sources of dissipation with classical shock waves as well known examples. To address this issue we need to write the integral energy balance equation

$$\sigma v|_{-\infty}^{+\infty} + V\Delta - \frac{d}{dt} \int_{-\infty}^{\infty} \left[\frac{v^2}{2} + \phi(\varepsilon) \right] = GV, \quad (2.4)$$

where $G(V) = [[\phi(\varepsilon)]] - \{\sigma(\varepsilon)\}[[\varepsilon]]$ is the driving/configurational force acting on the discontinuity, $\{f\} = (f_+ + f_-)/2$, and we assumed for determinacy that the body is infinite [24]. Note the unusual term $V\Delta$ which stands for the work performed by the *active agency* in transforming the system from passive to active state. Since our model is purely mechanical, the analog of the second law of thermodynamics, implying that the energy flux from macro-scale to micro-scale is irreversible, amounts to the requirement that

$$GV \geq 0, \quad (2.5)$$

which can serve as an additional (entropic) jump condition.

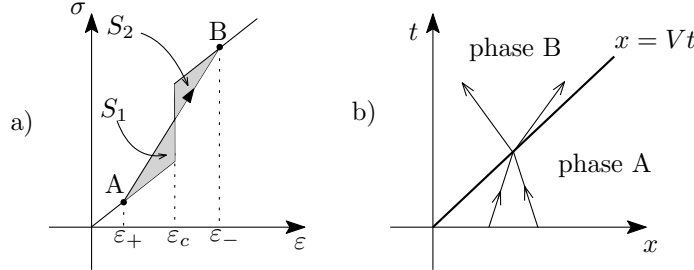


Figure 3: (a) The stress-strain relation crossed by the Rayleigh line $\sigma - \sigma_+ = \rho V^2(\varepsilon - \varepsilon_+)$ allows one to define the driving force as the area difference $G = S_2 - S_1$, (b) the (x, t) diagram showing the moving front interacting with two incoming and two outgoing characteristics.

To check whether the obtained set of jump conditions (2.3),(2.5) is sufficient, we need to specify the type of the discontinuity, see Fig. 3a). Consider the transition from a generic passive state A, with $\varepsilon = \varepsilon_+$, to the active state B, with $\varepsilon = \varepsilon_-$; the corresponding transformation front (strain discontinuity) traveling at a constant speed $V > 0$ transforms the state with the constant velocity $v = v_+$ to the state with the constant velocity $v = v_-$.

Note that the front AB is necessarily *supersonic* with respect to the state ahead of it, $V > c_+$, and is also *supersonic* with respect to state behind it, $V > c_-$, where we introduced the characteristic speeds $c_{\pm} = \sqrt{\sigma'(\varepsilon_{\pm})/\rho}$. Therefore, if we consider a point (x, t) which coincides with the current position of the front, two characteristics moving with velocities $\pm c_+$ will be coming to the front from the side of state A and two will be leaving to the side of state B, see Fig. 3b). Note also that for the classical phase boundaries, which are *subsonic* with respect to the state ahead and *subsonic* with respect to the state behind, there will be also two coming and two leaving characteristics, even though one of the coming characteristics will be arriving from behind, see [25]. In both cases, however, with two arriving characteristics, two Rankine-Hugoniot jump conditions (2.3), and the condition (2.4) being just an inequality, we do not have enough data to specify the 5 unknown parameters: states ahead and behind, $(\varepsilon_{\pm}, v_{\pm})$, plus the velocity of the discontinuity V .

To find the missing condition, which ultimately selects the velocity of the front, we need to solve the corresponding microscopic problem, which should allow one not only to confirm the non-negativity of the product GV but also to specify the *kinetic relation* $G = f(V)$.

3 Discrete model

Consider now the simplest mass-spring chain imitating the behavior of the continuum system (1.1). To this end we need to assume that the non-linear springs obey the force-elongation (stress-strain) relation $\sigma(\varepsilon)$ given by (2.2), see Fig. 1a). Suppose also that the equilibrium position of the masses are $x_n = na$ where a is the equilibrium spring length and n is an integer.

The dynamics of such FPU chain is governed by the equations:

$$\rho a \frac{d^2 u_n(t)}{dt^2} = \sigma \left(\frac{u_{n+1} - u_n}{a} \right) - \sigma \left(\frac{u_n - u_{n-1}}{a} \right), \quad (3.1)$$

where ρ is the mass density and $u_n(t)$ is the displacement of the n -th mass. Introducing the discrete strain $\varepsilon_n(t) = (u_{n+1}(t) - u_n(t))/a$, we can rewrite this system in the form:

$$\rho a^2 \frac{d^2 \varepsilon_n(t)}{dt^2} = \sigma(\varepsilon_{n+1}) + \sigma(\varepsilon_{n-1}) - 2\sigma(\varepsilon_n). \quad (3.2)$$

We are interested in the traveling wave (TW) solutions of the equations (3.2). We therefore assume that:

$$\varepsilon_n(t) = \varepsilon(\eta), \quad \varepsilon_{n\pm 1}(t) = \varepsilon(\eta \pm a), \quad \eta = na - Vt. \quad (3.3)$$

The point $\eta = 0$ will be associated with the position of the moving front.

If we non-dimensionalize the TW problem by introducing new variables:

$$\hat{V} = V/c, \quad \hat{\eta} = \eta/a, \quad \hat{\sigma} = \sigma/E, \quad \hat{\sigma}_0 = \sigma_0/E, \quad \hat{\phi} = \phi/E$$

and then drop the hats for simplicity, we obtain a single equation of motion in the form

$$V^2 \frac{d^2 \varepsilon}{d\eta^2} = \sigma(\eta + 1) + \sigma(\eta - 1) - 2\sigma(\eta). \quad (3.4)$$

where

$$\sigma(\eta) = \varepsilon(\eta) + \sigma_0 H(-\eta),$$

and $H(\eta)$ is the Heaviside function. For consistency with our stress-strain relations we need to supplement the equation (3.4) by the switching condition:

$$\varepsilon(0) = \varepsilon_c. \quad (3.5)$$

The transitional wave (kink) must also satisfy the following boundary conditions:

$$\varepsilon(\eta) = \begin{cases} \varepsilon_+, & \eta \rightarrow \infty, \\ \varepsilon_-, & \eta \rightarrow -\infty \end{cases} \quad (3.6)$$

The conditions (3.6) should be understood in the sense of averages in view of the possibility of the macroscopically invisible lattice wave oscillations carrying the energy away from the discontinuity [23].

It is natural to look for the solution of the problem in the form

$$\varepsilon(\eta) = \mathcal{E}(\eta) + \varepsilon_+$$

and instead of $\mathcal{E}(\eta)$ it will be more convenient to consider its Fourier transform

$$\check{\mathcal{E}}(p) = \int_{-\infty}^{\infty} \mathcal{E}(\eta) e^{ip\eta} d\eta.$$

In the Fourier space the equation (3.4) reduces to:

$$L(p)\check{\mathcal{E}}(p) = -\sigma_0 \frac{\omega^2(p)}{(0+ip)}, \quad (3.7)$$

where

$$L(p) = \omega^2(p) - (pV)^2 \quad (3.8)$$

is the Fourier image of the linear operator describing dynamics in each of the phases and

$$\omega^2(p) = 4 \sin^2\left(\frac{p}{2}\right) \quad (3.9)$$

is the dispersion relation in the linearized model. The denominator $(0+ip)$ in (3.7) comes from the Fourier transform of the Heaviside function and should be understood as $\lim_{\alpha \rightarrow 0+} (\alpha + ip)$. In what follows we write directly ip instead of $0 + ip$ keeping in mind that the singularity at $p = 0$ should be understood in the sense of the above limit.

The solution of (3.7) is straightforward and by inverting the Fourier transform we obtain

$$\varepsilon(\eta) = \varepsilon_+ - \frac{\sigma_0}{2\pi i} \int_{-\infty}^{\infty} \frac{\omega^2(p)}{L(p)} \frac{e^{-ip\eta}}{p} dp. \quad (3.10)$$

To evaluate the integral in (3.10) we can use the residue theorem. Due to symmetry, purely imaginary

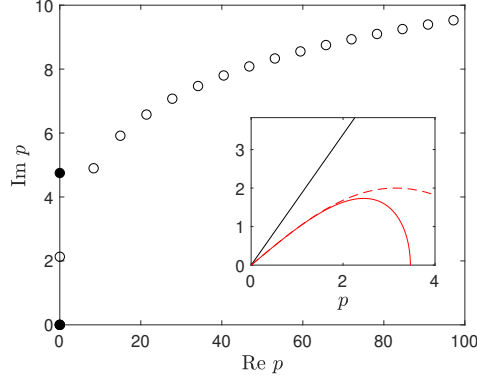


Figure 4: Zeros of the function $L(p)$, see (3.8), inside the first quadrant for the discrete (hollow circles) and quasi-continuum (filled circles) models. The inset shows the dispersion relation $\omega(p)$, for the discrete (red dashed line), see (3.9), and quasi-continuum (red solid line), see (4.5), models in relation to the line $\omega = Vp$ (black solid line).

roots of the function $L(p)$ appear in pairs while complex roots appear in quadruplets [19]. Since $V > 1$, the curves $\omega(p)$ and Vp have no intersections except at $p = 0$ and the real roots are absent (Fig. 4).

To specify the function $\varepsilon(\eta)$ we need to introduce the following sets

$$Z^{\pm} = \{p : L(p) = 0, \pm \text{Im } p > 0\}. \quad (3.11)$$

We can then write the explicit solution of the problem in the form

$$\varepsilon(\eta) = \begin{cases} \varepsilon_+ + \sum_{p_j \in Z^-} \frac{\sigma_0 \omega^2(p_j)}{p_j L'(p_j)} e^{-ip_j \eta}, & \eta > 0, \\ \varepsilon_+ + \frac{\sigma_0}{V^2 - 1} - \sum_{p_j \in Z^+} \frac{\sigma_0 \omega^2(p_j)}{p_j L'(p_j)} e^{-ip_j \eta}, & \eta < 0. \end{cases} \quad (3.12)$$

where we used the fact that the point $p = 0$ should be passed by the integration contour from below, see [19] for more details.

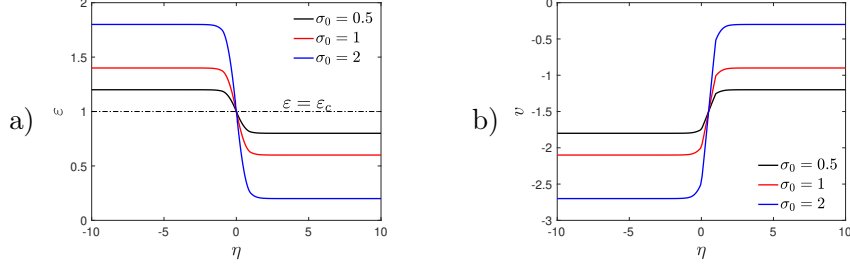


Figure 5: Strain (a) and velocity (b) profiles at $V = 1.5$ and different σ_0 .

The typical strain profiles are shown in Fig. 5a); these solutions are admissible in the sense that the critical strain is passed only once. To find the velocity distribution $v(\eta)$ we need to solve the equation $v(\eta) = -V du(\eta)/d\eta$, which in the Fourier space reads

$$\check{V}(p) = -V e^{ip/2} \frac{p/2}{\sin(p/2)} [2\pi\epsilon_+\delta(p) + \check{\mathcal{E}}(p)]. \quad (3.13)$$

In the real space we obtain (see Fig. 5b))

$$v(\eta) = \begin{cases} -V\epsilon_+ - \frac{V}{2} \sum_{p_j \in Z^-} \frac{\sigma_0 \omega^2(p_j)}{\sin(p_j/2) L'(p_j)} e^{-ip_j(\eta-1/2)}, & \eta > 1/2, \\ -V\epsilon_- + \frac{V}{2} \sum_{p_j \in Z^+} \frac{\sigma_0 \omega^2(p_j)}{\sin(p_j/2) L'(p_j)} e^{-ip_j(\eta-1/2)}, & \eta < 1/2. \end{cases} \quad (3.14)$$

The typical velocity profiles are shown in Fig. 5b). Finally, to obtain the displacement field $u(\eta)$ we need to solve the equation $\epsilon(\eta) = u(\eta + 1) - u(\eta)$. We can again use the Fourier transform to rewrite this equation in the form:

$$\check{U}(p) = \frac{i/2}{\sin(p/2)} (2\pi\epsilon_+\delta(p) + \check{\mathcal{E}}(p)) \quad (3.15)$$

By inverting the Fourier transform we obtain

$$u(\eta) = \begin{cases} \epsilon_+\eta + \frac{i}{2} \sum_{p_j \in Z^-} \frac{\sigma_0 \omega^2(p_j)}{p_j \sin(p_j/2) L'(p_j)} e^{-ip_j(\eta-1/2)}, & \eta > 1/2, \\ \epsilon_-\eta - \frac{\sigma_0}{2(V^2-1)} - \frac{i}{2} \sum_{p_j \in Z^+} \frac{\sigma_0 \omega^2(p_j)}{p_j \sin(p_j/2) L'(p_j)} e^{-ip_j(\eta-1/2)}, & \eta < 1/2. \end{cases} \quad (3.16)$$

where the linear term is due to a double pole at $p = 0$; an additive constant here is set to 0. The resulting particle trajectories are illustrated in Fig. 6 for the case when $\epsilon_+ = 0$ and $v_+ = 0$.

To compare the discrete solution (3.12, 3.14, 3.16) with its piecewise constant continuum counterpart, we first note that by considering the limit $\eta \rightarrow \pm\infty$ in (3.14) we obtain $v_{\pm} = -V\epsilon_{\pm}$, which can be rewritten as the first Rankine-Hugoniot condition (2.3): $\llbracket v \rrbracket = -V\llbracket \epsilon \rrbracket$. Note also that the conditions (3.6) are fulfilled if

$$\epsilon_- = \epsilon_+ + \frac{\sigma_0}{V^2-1}. \quad (3.17)$$

which can be rewritten as the second Rankine-Hugoniot condition: $V^2\llbracket \epsilon \rrbracket - \llbracket \sigma(\epsilon) \rrbracket = 0$.

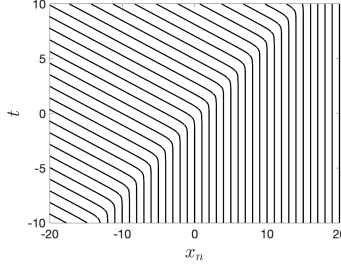


Figure 6: Trajectories of mass points $x_n(t) = n + u_n(t)$ for the kink moving with the velocity $V = \sqrt{2}$; $\sigma_0 = 2$.

Finally, we can use (3.5) to obtain the selection condition for the discontinuity velocity V (kinetic relation). If we integrate $\omega^2(p)/(pL(p))$ over the circle with the radius expanding to infinity and apply the residue theorem, we obtain

$$\sum_{p_j \in Z} \frac{\omega^2(p_j)}{p_j L'(p_j)} = \frac{1}{V^2 - 1}, \quad (3.18)$$

where the sum is taken over all zeros of $L(p)$. Hence, the continuity of $\varepsilon(\eta)$ at the point $\eta = 0$ holds and the value $\varepsilon(0) = \varepsilon_c$ can be obtained by considering for instance the limit $\eta \rightarrow +0$ in (3.12). Moreover, due to the symmetry of the roots we obtain

$$\sum_{p_j \in Z^+} \frac{\omega^2(p_j)}{p_j L'(p_j)} = \sum_{p_j \in Z^-} \frac{\omega^2(p_j)}{p_j L'(p_j)} \quad (3.19)$$

which allows us to rewrite the condition (3.5) in the form

$$\varepsilon_+ = \varepsilon_c - \frac{1}{2} \frac{\sigma_0}{V^2 - 1}. \quad (3.20)$$

Equation (3.20) is the desired kinetic relation. It is easy to check that it is equivalent to the trivial condition

$$G(V) = 0. \quad (3.21)$$

In other words, the magnitude of the driving force always takes the lowest possible value (equal to zero) and as a result the constructed solutions are dissipation free. Therefore, all the energy provided by the active agency (which can be also interpreted as anti-dissipation) is consumed by the transformation itself. The absence of the radiative damping in the form of emitted lattice-scale waves is the consequence of the supersonic nature of the transition which effectively *overtakes* any emitted acoustic wave.

To check stability of the obtained solutions we performed numerical integration of the initial value problem for the system (3.2) with $N = 2000$ springs, $\varepsilon_c = 1$ and $\sigma_0 = 2$. In the first type of tests we considered the Riemann problem with initial conditions:

$$\left(\varepsilon_n(0), \frac{d\varepsilon_n}{dt}(0) \right) = \begin{cases} (\varepsilon_l, 0), & n < 1000, \\ (\varepsilon_c, 0), & n = 1000, \\ (\varepsilon_r, 0), & n > 1000, \end{cases} \quad (3.22)$$

where ε_l and ε_r are constants, while keeping both ends of the chain free. The results of a typical simulation of this type are illustrated in Fig. 7 where we show the time section $t = 600$ when all the fronts have sufficiently stabilized. We observe the emergence of a steadily moving transition front AB whose internal structure is in excellent agreement with the analytical solution (3.14), see the right inset in Fig. 7. The

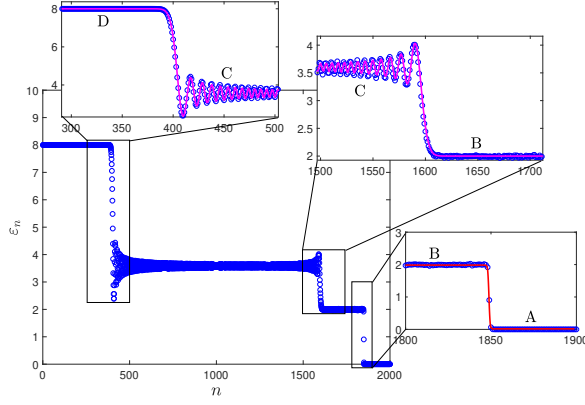


Figure 7: Results of numerical simulations with the Riemann initial conditions $(\varepsilon_l, \varepsilon_r) = (8, 0)$ at $t = 600$. The steady-state solutions in the right zoomed area is compared with the analytical solution (3.12) (solid red line). The remaining inserts show expanding sonic waves matched with the theoretical solution (A.2) (solid magenta lines). Different states A, B, C and D are indicated in the insets.

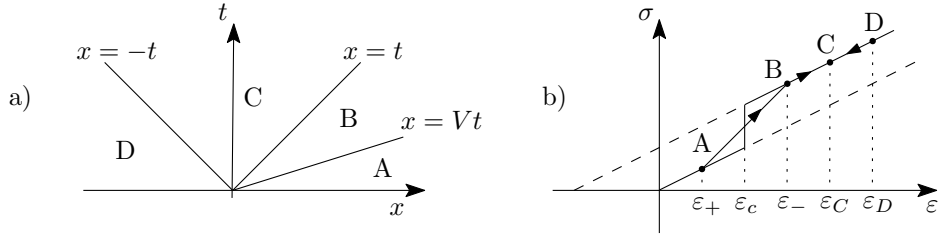


Figure 8: Breakdown of unstable piecewise constant initial state (Riemann problem): (a) Propagating supersonic front of nonlinear (passive-active) transformation and two 'supporting' the sonic waves, (b) Global structure of the solution of the Riemann problem. The analytical solutions (3.12) (solid red line) and (A.2) (solid magenta line) are shown in insets for comparison.

steady-state traveling wave propagates with the velocity $V = 1.42$ which is independent of the initial value ε_l once we fixed $\varepsilon_r = 0$.

Note the presence of two spreading sonic waves (BC and DC) which move in the opposite directions with the same speed $V = 1$. Their internal structure is reconstructed analytically in appendix A and our two other insets show an excellent agreement between the theory and the numerical experiment.

To interpret the global structure of the solution of this Riemann problem we show in Fig. 8a) the spatial configuration of the all three propagating fronts. The nonlinear transition AB and the linear transitions BC and CD are also illustrated on the stress-strain curve in Fig. 8b) where the average strains in the points A and B are ε_+ and ε_- , respectively; within the active phase, we observe two strain plateaus at ε_C and $\varepsilon_D = \varepsilon_l$.

We also performed another type of numerical experiment where we solved equations (3.1) with homogeneous initial conditions $u_n(0), du_n(0)/dt = 0$ for any n , while keeping the right end of the chain free and applying a constant force F at its left end:

$$\left(u_n(0), \frac{du_n}{dt}(0)\right) = (0, 0), \quad \frac{d^2 u_1}{dt^2} = \sigma(\varepsilon_1) - F. \quad (3.23)$$

The results of these simulations with $F = 5$ and the other parameters as in the first set of tests are summarized in Fig. 9. We again observe the formation of the transformation front AB moving with velocity $V = 1.42$ and we have checked that this value does not depend on the magnitude of the applied force. The inset on the right in Fig. 9 shows an excellent agreement between numerical and analytical

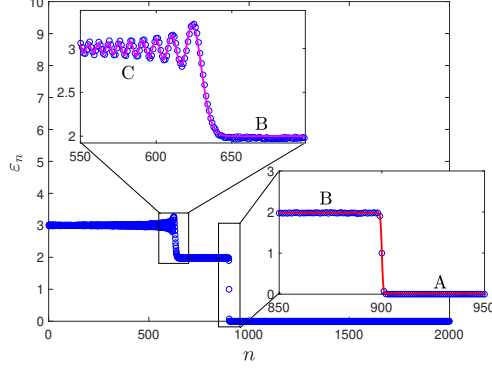


Figure 9: Snapshot of the numerical solution of the initial value problem with externally applied force $F = 5$. Here $t = 634$ when the first 900 switching transitions occurred. The analytical solutions (3.12) (solid red line) and (A.2) (solid magenta line) are shown in insets for comparison.

results. As in our other tests the formation of this nonlinear front is 'compensated' by the formation of a linear wave which propagates with $V = 1$ and $\varepsilon_C = F - \sigma_0$ and whose structure is analytically characterized in appendix A.

4 Quasi-continuum model

It is of interest to check to what extent the simplest mesoscopic quasi-continuum model, providing only a long wavelength approximation of the microscopic discrete solution, and capturing only some of its dispersive properties, is compatible with the obtained lattice scale solution.

If we use the first nontrivial term in the Fourier space polynomial expansion of the linear operator involved in the formulation of the discrete theory [21, 23] we obtain a continuum model with the elastic energy 'corrected' by the strain gradient term. The kinetic energy remains the same as in conventional continuum theory and the total energy can be written in the form

$$\mathcal{U} = \int_{-\infty}^{\infty} \left[\frac{\rho v^2}{2} + \phi(\varepsilon) - \frac{Ea^2}{12} \left(\frac{\partial \varepsilon}{\partial x} \right)^2 \right] dx \quad (4.1)$$

where the factor $a^2/12$ reflects the fact that the discrete model contained nearest neighbor interactions only [26]. Note that the strain gradient term appears with the negative sign which makes the model (4.1) unstable with respect to perturbations with sufficiently small wave lengths. However, such unstable wave lengths will be absent in the solutions obtained below which suggests that the predictions of this model can still be trusted.

The quasi-continuum analog of the equation (1.1) takes the form

$$\rho \frac{\partial^2 u(x, t)}{\partial t^2} = \frac{\partial \sigma(\varepsilon)}{\partial x} + \frac{Ea^2}{12} \frac{\partial^4 u(x, t)}{\partial x^4}, \quad (4.2)$$

where the dependence $\sigma = \sigma(\varepsilon)$ is given by (2.2). If we nondimensionalize (4.2) and limit our attention to traveling waves we obtain

$$V^2 \frac{d^2 \varepsilon(\eta)}{d\eta^2} = \frac{d^2 \sigma(\eta)}{d\eta^2} + \frac{1}{12} \frac{d^4 \varepsilon(\eta)}{d\eta^4}. \quad (4.3)$$

The solution of this equation can be again obtained using the Fourier transform

$$\varepsilon(\eta) = \varepsilon_+ + \frac{\sigma_0}{2\pi i} \int_{-\infty}^{\infty} \frac{12}{(p + iz)(p - iz)} \frac{e^{-ip\eta}}{p} dp \quad (4.4)$$

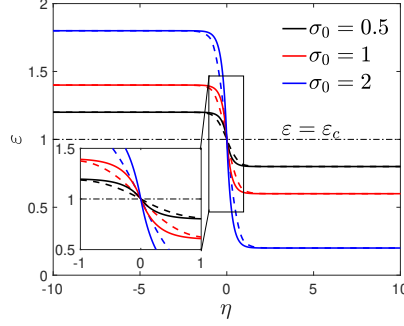


Figure 10: Quasi-continuum profile of the transformation front at $V = 1.5$ and different σ_0 (solid lines). The dashed lines show corresponding solutions of the discrete problem.

where $z = \sqrt{12(V^2 - 1)}$. To compute the integral in (4.4) we can again apply the residue theorem remembering that the point $p = 0$ should be passed from below. In this case we have to deal with much simpler dispersion relation

$$\omega^2(p) = p^2 - p^4/12. \quad (4.5)$$

As a result, the only three singularities of the denominator in (4.4) are at $p = 0$ and $p = \pm iz$, see Fig. 4. The solution can be then written explicitly

$$\varepsilon(\eta) = \begin{cases} \varepsilon_+ + \frac{\sigma_0}{2} \frac{1}{V^2 - 1} e^{-z\eta}, & \eta > 0 \\ \varepsilon_+ + \frac{\sigma_0}{V^2 - 1} - \frac{\sigma_0}{2} \frac{1}{V^2 - 1} e^{z\eta}, & \eta < 0, \end{cases} \quad (4.6)$$

One can check that the average strains are related again through the RH condition: $\varepsilon_- = \varepsilon_+ + \sigma_0/(V^2 - 1)$. To find the velocity distribution we can use the equation $v(\eta) = -V\varepsilon(\eta)$ which gives:

$$v(\eta) = \begin{cases} -V\varepsilon_+ - \frac{\sigma_0}{2} \frac{V}{V^2 - 1} e^{-z\eta}, & \eta > 0, \\ -V\varepsilon_- + \frac{\sigma_0}{2} \frac{V}{V^2 - 1} e^{z\eta}, & \eta < 0. \end{cases} \quad (4.7)$$

The second RH condition is now satisfied automatically.

If we now require the solution (4.6) to meet the switching condition at $\eta = 0$ we obtain the same (trivial) kinetic relation as in the discrete case, $G(V) = 0$. The absence of dissipation is again due to the supersonic nature of our kinks: this leads to the absence of real roots of the quasi-continuum characteristic relation which could describe linear waves carrying energy away from the moving kink.

Examples of the quasi-continuum strain profiles at $V = 1.5$ are shown in Fig. 10 by solid lines. In the same figure we also show the associated solutions of the discrete problem (dashed lines). The inset illustrates the mismatch which is visible only in the immediate vicinity of the origin.

We can conclude that the quasi-continuum description of the supersonic active kinks based on (4.2) is fully adequate and is missing only the fine details of the structure of the core region of the moving front. We recall that to capture these fine details we needed to account for the infinite number of the complex roots of the discrete characteristic equation. Also recall that the corresponding fully adequate solution was obtained in the form of infinite series. Instead, the quasi-continuum solution, which relies only on a small number of roots, captures the main features of the discrete model while remaining not only explicit but also extremely simple. Similarly remarkable efficiency of the simple quasi-continuum approximations in the description of supersonic solitons in discrete chains was shown in [27].

5 Active solitary waves

To further illustrate the discrete model we now construct analytically approximate solitary wave solutions describing autonomously propagating activity bands. We then demonstrate numerically that such solutions exhibit some of the collision features characteristic of actual solitons.

Observe that in view of its non-dissipative nature, the frontal kink, transforming a passive state into an active state and sustained by an internal source with intensity $\Delta > 0$, can be in principle followed by a symmetry related, equally non-dissipative rear anti-kink which requires for its propagation the energy removal performed by an internal sink with intensity $-\Delta < 0$. We assume that such sources and sinks are present: the discussion of their micro-realization goes beyond the scope in this paper.

More specifically, in § 3 we obtained a traveling wave solution describing the transition from the state A to the state B which advances at velocity V . We can now construct a traveling wave solution describing transition from B to A which moves with the same velocity. The constants in the boundary conditions (3.6) should be simply swapped and we obtain the following relations for the strain field

$$\varepsilon(\eta) = \begin{cases} \varepsilon_- - \sum_{p_j \in Z^-} \frac{\sigma_0 \omega^2(p_j)}{p_j L'(p_j)} e^{-ip_j \eta}, & \eta > 0, \\ \varepsilon_+ + \sum_{p_j \in Z^+} \frac{\sigma_0 \omega^2(p_j)}{p_j L'(p_j)} e^{-ip_j \eta}, & \eta < 0, \end{cases} \quad (5.1)$$

the velocity field

$$v(\eta) = \begin{cases} -V\varepsilon_- + \frac{V}{2} \sum_{p_j \in Z^-} \frac{\sigma_0 \omega^2(p_j)}{\sin(p_j/2) L'(p_j)} e^{-ip_j(\eta-1/2)}, & \eta > 1/2, \\ -V\varepsilon_+ - \frac{V}{2} \sum_{p_j \in Z^+} \frac{\sigma_0 \omega^2(p_j)}{\sin(p_j/2) L'(p_j)} e^{-ip_j(\eta-1/2)}, & \eta < 1/2, \end{cases} \quad (5.2)$$

and the displacement field

$$u(\eta) = \begin{cases} \varepsilon_- \eta + \frac{\sigma_0}{2(V^2 - 1)} - \frac{i}{2} \sum_{p_j \in Z^-} \frac{\sigma_0 \omega^2(p_j)}{p_j \sin(p_j/2) L'(p_j)} e^{-ip_j(\eta-1/2)}, & \eta > 1/2, \\ \varepsilon_+ \eta + \frac{i}{2} \sum_{p_j \in Z^+} \frac{\sigma_0 \omega^2(p_j)}{p_j \sin(p_j/2) L'(p_j)} e^{-ip_j(\eta-1/2)}, & \eta < 1/2. \end{cases} \quad (5.3)$$

The equation of the energy balance (2.4) takes the form:

$$\sigma v|_{-\infty}^{+\infty} - V\Delta - \frac{d}{dt} \int_{-\infty}^{\infty} \left[\frac{v^2}{2} + \phi(\varepsilon) \right] = GV. \quad (5.4)$$

Note that the active energy source transformed here into the energy sink; the kinetic equation here is again $G(V) = 0$.

If we now assume that the transition AB takes place at the value of the TW coordinate $\eta = d$ and that the reverse transition BA takes place at $\eta = -d$, and that in (3.4) the right-hand side has been changed to $\sigma(\eta) = \varepsilon(\eta) + \sigma_0 [H(d - \eta) - H(d + \eta)]$, the approximate solitary wave solution can be written as a simple superposition of the corresponding kink and anti-kink solutions:

$$\begin{aligned} \varepsilon_s(\eta) &= \varepsilon_+ + \varepsilon(\eta - d) - \varepsilon(\eta + d), \\ v_s(\eta) &= v_+ + v(\eta - d) - v(\eta + d), \\ u_s(\eta) &= \varepsilon_+ \eta + u(\eta - d) - u(\eta + d). \end{aligned} \quad (5.5)$$

Here the functions $\varepsilon(\eta)$, $v(\eta)$ and $u(\eta)$ are given by (3.12), (3.14) and (3.16); the constant ε_+ is given again by (3.20).

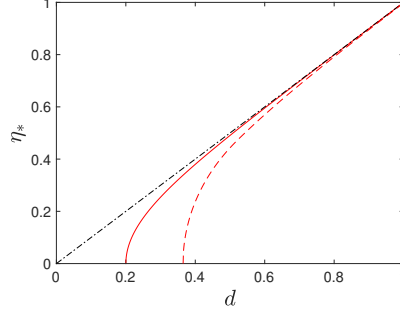


Figure 11: Solutions of the equation $\varepsilon_s(\eta_*) = \varepsilon_c$ for the discrete (red dashed line) and quasi-continuum (red solid line) models with $V = \sqrt{2}$, $\varepsilon_c = 1$, $\sigma_0 = 2$. The straight black dash-dotted line is $\eta_* = d$.

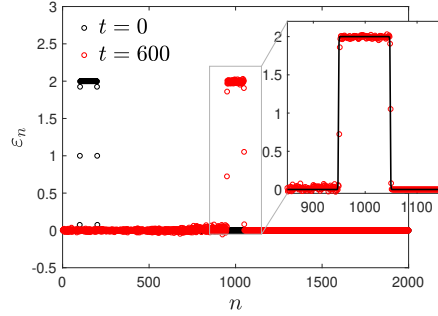


Figure 12: Snapshots at $t = 0$ and $t = 600$ of the soliton-type solution with the half-width $d = 50$ propagating at the speed $V = \sqrt{2}$. The inset compares the initial and the current configurations.

Suppose next that we fix d and solve the algebraic equation $\varepsilon_s(\eta_*) = \varepsilon_c$ obtaining the relation $\eta_*(d)$. The traveling wave (5.5) is an exact solution if there exists a value of d such that $\eta_*(d) = d$. The function $\eta_* = \eta_*(d)$ computed numerically is shown in Fig. 11 (red dashed line) where we also present its quasicontinuum analog (red solid line) which is known analytically

$$\eta_* = z^{-1} \cosh^{-1} \left((\varepsilon_c - \varepsilon_+) \left[1 - \frac{V^2 - 1}{\sigma_0} \right] \exp(zd) \right), \quad (5.6)$$

and where $z = \sqrt{12(V^2 - 1)}$. While none of these curves crosses the straight line $\eta = d$, they become close at large d which suggests that in this range of parameters the approximate configuration (5.5) will evolve towards the actual solitary wave type solution (if it exists).

To check the actual existence of such solitary waves, we resolve to numerical simulations. We take the ansatz (5.5) as our initial data, keep the parameters $\sigma_0 = 2$, $\varepsilon_c = 1$ as in our previous numerical simulations and set $V = \sqrt{2}$ which results in $\varepsilon_+ = 0$.

If we choose initial perturbation with small $d \sim 1$, when the approximation is expected to be poor, the ensuing dynamics shows de-localization of the pulse with fast decay of its amplitude.

If, instead, the initial pulse is wide with $d \sim 50$ its evolution is completely different, see Fig. 12. Our numerical simulations show a steadily propagating solitary wave with the speed anticipated by our analytical approximation even though we also observe some noise left in the wake. We can conjecture that even if initially localized energy eventually dissipates into small scale oscillations, it would take considerable time. Note that the resulting motion, see Fig. 13, is supported exclusively by the internal activity which effectively *translocates* the particles to the left by ~ 200 units.

Finally, to show that the obtained solitary wave type solutions have some properties of actual solitons, we performed the collision between two such waves with half-width $d = 50$ moving against each other with

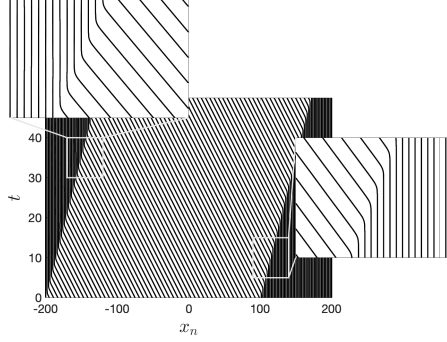


Figure 13: Particle motion $x_n(t) = n + u_n(t)$ associated with the soliton-type solution shown in Fig. 12 for $n = 100, 102, 104, \dots, 200$.

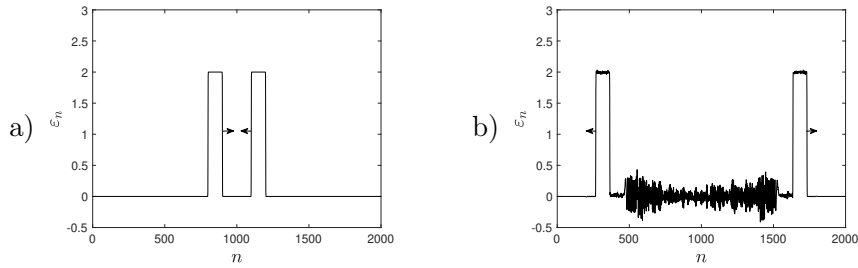


Figure 14: Quasi-elastic collision of two solitary waves with half-width $d = 50$ and speed $V = \sqrt{2}$: a) before the collision at $t = 0$, b) after the collision at $t = 600$. Arrows indicate the propagation directions.

velocities $V = \pm\sqrt{2}$, see Fig. 14. We observe that despite almost elastic interaction, a very limited amount of energy is lost because of the formation of small scale oscillations. In the Supplementary Material we included the animation showing that during the collision, taking place between $t \approx 60$ and $t \approx 150$, there is a considerable increase of strain which then subsides to the values prescribed by the initial data.

6 Conclusions

We used the simplest model of an active solid to obtain an analytical description of a propagating front which transform a passive phase (no active stress) into an active phase (active stress is present). Inertial effects were taken into consideration because the targeted solids are expected to be anomalously *soft*.

We assumed that the steady advancement of such fronts can be self-sustained in the sense that it can be fuelled by an internal energy reservoir presenting itself as an effective source of *anti-dissipation*. In various biological settings the implied activity is revealed through the work done, for instance, by the macroscopically invisible molecular motors. Our conclusion that the transformation fronts must be necessarily supersonic is meaningful because in biologically relevant active solids the acoustic speeds may be arbitrarily small.

As we showed, the supersonic nature of the transformation fronts eliminates the possibility of the radiative damping which is an important source of dissipation for classical defects in crystalline solids. Such purely mechanical dissipation can be therefore neglected in the case of propagating activity fronts which emerge as largely anti-dissipative.

We presented three different descriptions of such transformation fronts: continuum, discrete and quasicontinuum. The classical continuum model is not self-contained because the condition of non-dissipativeness has to be added phenomenologically. Instead, both discrete and quasi-continuum models

provide this supplementary condition automatically.

Since our discrete model basically coincides with the well known FPU system, we effectively generalized the latter to the case when springs can be both passive and active, allowing for the propagation of active phase transition fronts. Our ability to construct quasi-continuum solutions reproducing faithfully all the properties as the discrete solution shows that the complexity of the dispersion relations exhibited by the discrete system is not necessary for capturing the observed behavior which can be already reproduced using the simplest polynomial approximation of the discrete dispersion relation. Our quasi-continuum approximation coincides with the 'bad Boussinesque' model which is generically unstable but works in our case since the obtained solution is confined to a finite ball in the Fourier space where the implied instability is absent.

From the perspective of the theory of nonlinear waves in dispersive systems the obtained kink type solutions are special in the sense that the discreteness of the structure does not automatically lead to lattice resonances and the associated dissipation. Such nondissipative propagation of lattice ways is sometimes interpreted as lattice transparency. While in subsonic case such regimes require very particular conditions, in the supersonic case they become robust.

Funding

NG acknowledges the support of the French Agence Nationale de la Recherche (ANR) under reference ANR-17-CE08-0047-02. LT was supported by the grant ANR-10-IDEX-0001-02 PSL.

Acknowledgements

We dedicate this work to the 90th birthday of Leonid Slepyan, an amazing scientist and a truly great man.

A Appendix

Following [28], we consider the linear problem (no transition). We start with the solution for the semi-infinite domain which can be obtained by solving the problem symmetric loading

$$\frac{d^2 u(x, t)}{dt^2} = u(x + 1, t) + u(x - 1, t) - 2u(x, t) - \delta(x - 1) - \delta(x), \quad -\infty < x < \infty, \quad (\text{A.1})$$

and then taking $x \geq 1$. It is implied here that the initial conditions are trivial: $u(x, 0) = 0, du(x, 0)/dt = 0$. Because of the symmetry $\varepsilon(1, t) = u(1, t) - u(0, t) = 0$ and by inverting the discrete Fourier transform, we obtain the desired solution

$$\varepsilon(x, t) = \frac{2}{\pi} \int_0^{\pi/2} \frac{\cos p}{\sin p} (1 - \cos(2t \sin p)) \sin 2px \, dp. \quad (\text{A.2})$$

To match the transitions BC or DC shown in Fig. 7 and Fig. 9, we need to multiply (A.2) by the appropriate factor and adjust the shift, for instance, to match the transition BC in Fig. 7 we need to use the multiple $(\varepsilon_C - \varepsilon_+)$ and the additive term ε_+ . After these adjustments we obtain the profiles shown in the insets in Fig. 7 and Fig. 9 (magenta lines).

To obtain analytical results we need to study the integral in (A.2) in the limit $t \rightarrow \infty$, see also [28, sec. I]. We first rewrite it in the form:

$$\begin{aligned} \varepsilon(x, t) = & -\frac{1}{\pi} \int_0^{\pi/2} \frac{\cos p}{\sin p} [\sin(2(px + t \sin p)) + \sin(2(px - t \sin p))] \, dp \\ & + \frac{2}{\pi} \int_0^{\pi/2} \frac{\cos p}{\sin p} \sin 2px \, dp. \end{aligned} \quad (\text{A.3})$$

The time evolution is contained in the first integral where the phases $px + t \sin p$ and $px - t \sin p$ describe waves propagating in the negative and positive x directions, respectively. The last integral is the irrelevant time independent term.

In the limit $t \rightarrow \infty$ the major contribution to the integral comes from the end points of the interval and at stationary points of the phases. However, the integrand is zero at $p = \pi/2$ due to the presence of the term $\cos p$. Moreover, the stationary points $p_{1,2}$ are such that $\cos p_{1,2} = \pm p/t$. This becomes $\pm \pi/2$ in the limit $t \rightarrow \infty$ and, hence, the contribution of these terms is minor. Therefore, it is sufficient to account for the contribution to the integral from the points close to $p = 0$:

$$\varepsilon(x, t) \sim -\frac{1}{\pi} \int_0^\delta \frac{\sin(2(px + t \sin p)) + \sin(2(px - t \sin p))}{p} dp, \quad t \rightarrow \infty \quad (\text{A.4})$$

where we introduced the small parameter $\delta \ll 1$. If $|x \pm t| \geq t^a$, $a > 1/3$, we can make the change of variables $y = p(x \pm t)$. Then in the limit $t \rightarrow \infty$ the upper integration limit becomes infinity and the integrals converge to $\pi/2 \text{sign}(x \pm t)$.

A different result is obtained when $|x \pm t| = O(t^{1/3})$. Making the change of variables $z = pt^{1/3}$ in the integral and setting $\delta t^{1/3} \rightarrow \infty$ we get:

$$\int_0^\delta \frac{\sin(2(x \pm t)p \mp p^3 t/3)}{p} = \int_0^\infty \frac{\sin(\xi^\pm z \mp z^3/3)}{z} dz, \quad \xi^\pm = 2 \frac{x \pm t}{t^{1/3}} \quad (\text{A.5})$$

From these expressions we see that the sonic wave propagates with velocity $V = 1$ and its front spreading

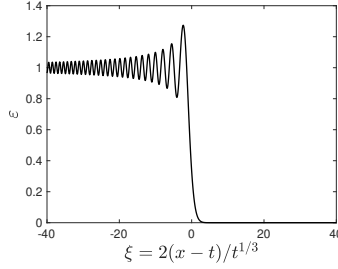


Figure 15: Asymptotic behaviour (A.7) for the sonic wave when $t \rightarrow \infty$.

follows the asymptotics $t^{1/3}$. More precisely, we can write

$$\varepsilon(x, t) \sim \int_{\xi^-}^\infty \text{Ai}(x) dx + \int_{\xi^+}^\infty \text{Ai}(-x) dx, \quad t \rightarrow \infty, \quad \text{Ai}(x) = \frac{1}{\pi} \int_0^\infty \cos\left(zx + \frac{z^3}{3}\right) dz, \quad (\text{A.6})$$

where $\text{Ai}(x)$ is the Airy function. Finally, by letting $\xi^+ \rightarrow \infty$, i.e. by switching to the moving frame ξ^- , we can make the second integral vanish and the asymptotic expression for strain takes a simple form:

$$\varepsilon(x, t) \sim \int_{\xi}^\infty \text{Ai}(x) dx, \quad t \rightarrow \infty, \quad \xi = 2 \frac{x - t}{t^{1/3}} \quad (\text{A.7})$$

Function (A.7) is plotted in Fig. 15. The obtained profile is the same as the ones emerging in our numerical simulations, see Fig. 7 and Fig. 9. The exact matching can be achieved by shifting the origin and adding the appropriate factor.

References

- [1] MC Marchetti, J-F Joanny, S Ramaswamy, TB Liverpool, J Prost, M Rao, and RA Simha. Hydrodynamics of soft active matter. *Reviews of Modern Physics*, 85(3):1143, 2013.
- [2] G De Magistris and D Marenduzzo. An introduction to the physics of active matter. *Physica A: Statistical Mechanics and its Applications*, 418:65–77, 2015.
- [3] É Fodor and MC Marchetti. The statistical physics of active matter: From self-catalytic colloids to living cells. *Physica A: Statistical Mechanics and its Applications*, 504:106–120, 2018.
- [4] L Berthier, E Flenner, and G Szamel. Glassy dynamics in dense systems of active particles. *The Journal of chemical physics*, 150(20):200901, 2019.
- [5] AP Solon, J-B Caussin, D Bartolo, H Chaté, and J Tailleur. Pattern formation in flocking models: A hydrodynamic description. *Physical Review E*, 92(6):062111, 2015.
- [6] W Ngamsaad and S Suantai. Propagating wave in the flock of self-propelled particles. *Physical Review E*, 98(6):062618, 2018.
- [7] J Prost, F Jülicher, and J-F Joanny. Active gel physics. *Nature Physics*, 11(2):111, 2015.
- [8] F Jülicher, SW Grill, and G Salbreux. Hydrodynamic theory of active matter. *Reports on Progress in Physics*, 81(7):076601, 2018.
- [9] RJ Hawkins and TB Liverpool. Stress reorganization and response in active solids. *Physical review letters*, 113(2):028102, 2014.
- [10] A Maitra and S Ramaswamy. Oriented active solids. *arXiv preprint arXiv:1812.01374*, 2018.
- [11] M Moshe, MJ Bowick, and MC Marchetti. Geometric frustration and solid-solid transitions in model 2D tissue. *Physical review letters*, 120(26):268105, 2018.
- [12] C Scheibner, A Souslov, D Banerjee, P Surowka, W Irvine, and V Vitelli. Odd elasticity in active metamaterials. *arXiv preprint arXiv:1902.07760*, 2019.
- [13] BA Finlayson and LE Scriven. Convective instability by active stress. *Proceedings of the Royal Society of London. A. Mathematical and Physical Sciences*, 310(1501):183–219, 1969.
- [14] JE Cohen and P Horowitz. Paradoxical behaviour of mechanical and electrical networks. *Nature*, 352(6337):699, 1991.
- [15] D Braess. Über ein paradoxon aus der verkehrsplanung. *Unternehmensforschung*, 12(1):258–268, 1968.
- [16] ZG Nicolaou and AE Motter. Mechanical metamaterials with negative compressibility transitions. *Nature materials*, 11(7):608, 2012.
- [17] M Ayzenberg-Stepanenko, G Mishuris, and L Slepyan. Brittle fracture in a periodic structure with internal potential energy. spontaneous crack propagation. *Proceedings of the Royal Society A: Mathematical, Physical and Engineering Sciences*, 470(2167):20140121, 2014.
- [18] G Gallavotti. *The Fermi-Pasta-Ulam problem: a status report*, volume 728. Springer, 2007.
- [19] L Truskinovsky and A Vainchtein. Kinetics of martensitic phase transitions: lattice model. *SIAM Journal on Applied Mathematics*, 66(2):533–553, 2005.

- [20] L Slepyan, A Cherkaev, and E Cherkaev. Transition waves in bistable structures. II. Analytical solution: wave speed and energy dissipation. *Journal of the Mechanics and Physics of Solids*, 53(2):407–436, 2005.
- [21] L Truskinovsky and A Vainchtein. Quasicontinuum models of dynamic phase transitions. *Continuum Mechanics and Thermodynamics*, 18(1-2):1–21, 2006.
- [22] LI Slepyan and LV Troyankina. Impact waves in a nonlinear chain. *Plasticity and Fracture of Solids*, pages 175–186, 1988. (In Russian).
- [23] LI Slepyan. *Models and phenomena in fracture mechanics*. Springer Science & Business Media, 2012.
- [24] L Truskinovskii. Dynamics of non-equilibrium phase boundaries in a heat conducting non-linearly elastic medium. *Journal of Applied Mathematics and Mechanics*, 51(6):777–784, 1987.
- [25] L Truskinovsky. Kinks versus shocks. In *Shock induced transitions and phase structures in general media*, pages 185–229. Springer, 1993.
- [26] RD Mindlin. Theories of elastic continua and crystal lattice theories. In *Mechanics of Generalized Continua*, pages 312–320. Springer, 1968.
- [27] L Truskinovsky and A Vainchtein. Solitary waves in a nonintegrable Fermi-Pasta-Ulam chain. *Physical Review E*, 90(4):042903, 2014.
- [28] LI Slepyan. Nonstationary elastic waves. *Sudostroenie, Leningrad*, page 376, 1972. (In Russian).